$$C_j = \sum_{i=j+\frac{b+1}{2}}^{j+a+\frac{b-1}{2}} S_i - \sum_{i=j-a-\frac{b-1}{2}}^{j-\frac{b+1}{2}} S_i \qquad (2)$$

The C_j function is evaluated in each point as the difference between the sum of the density values of the spectrum (S_i) within two windows symmetric to pixel j, having a pixels width and distant b pixels. We have tested that the values of $a = 5$, $b = 1$ provide the best results. This does not allow an accurate wavelength calibration, but the knowledge of the point in which the prism spectrum abruptly drops is essential for the subsequent fit of the continuum.

The use of density units and the different spectral distribution of all the objects does not allow to obtain a continuum pattern to be scaled and fitted to each spectrum. It is necessary to create a curve able to fit all type of spectra, but it also must point out the emission feature if this one exists. With this aim, a cubic spline curve was fitted from central to red region of the spectrum, the range where we will search for the line. An iterative process has been adopted, rejecting points 2 sigma over the calculated continuum. This procedure provides accurate continua for all the spectral shapes, including those with a strong emission line feature, as we show in Fig. 3.

3.4. *Analysis of the spectral shape*

In order to improve the efficiency of the selection procedure, we have analyzed the shape of the one-dimensional spectra. Each prism spectrum has been characterized by the slopes derived in three bands. Two of them have been chosen at both sides with respect to the point with higher signal, and the last one towards the blue end of the spectrum. Each band covers 10 pixels (about 200 Å) and a second order polynomial fit has been derived for each region. Figure 4 shows the three bands and the fits performed for a typical spectrum. The slopes are calculated in the middle of the blue band ($S1$) and in the pixel of higher signal ($S2, S3$) for the other two bands.

The variations in the slopes will show the distribution and the peculiarities of the prism spectra. In the absence of the Hα line in emission, they will show a smooth instrumental shape, with the two last bands located in the point of higher sensitivity of the IIIaF emulsion. In this case, we expect typical values of $S2 - S1 < 0$ and $S2 - S3 \approx 0$. If the spectrum presents the Hα line in emission, the two last bands will be located on the winds of the line, whereas the first band will show the continuum distribution. The emission line will produce a hard increase in density, high variations in the slope of the continuum and near the line, and strong discontinuities on the top of the line, that is, typical values of $S2 - S1 \gg 0$; $S2 - S3 \gg 0$.

4. Selection of candidates

Candidates of ELGs will be selected to present large differences in the measured parameters with those obtained for the majority of the objects. The criteria will be the existence of high residuals (R) between the extracted spectrum and the estimated continuum, and the presence of strong variations in the slope of the spectrum as exposed in the precedent point. In order to establish the typical values of R, $S2-S1$ and $S2-S3$, we have plotted these parameters versus the density fluxes for each object as shown in Figs. 5a-c. A curve has been fitted to the data following an iterative procedure in order to reject the contribution of points with the largest deviations. The plots show the final fits and the 3σ curve. We compute the difference, in sigma units, between the three measured parameters and those estimated using the fits, filtering the data imposing a minimum of 2σ in each deviation. Finally, we establish a selector index as the sum of these three deviations.

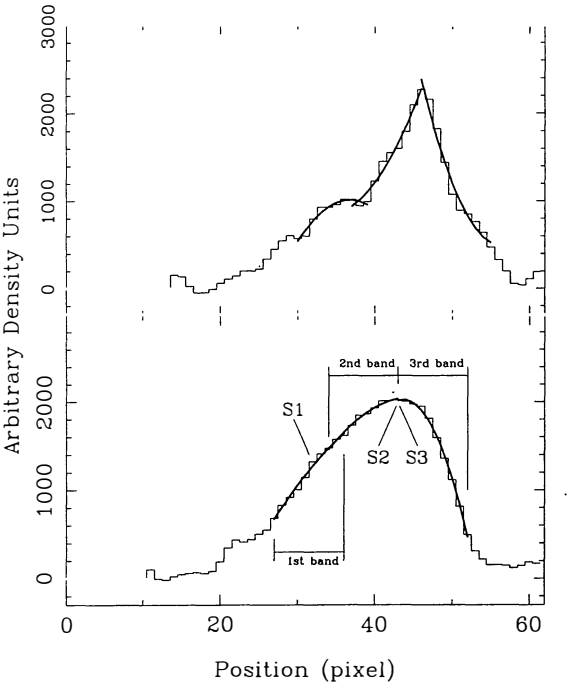

Fig. 4. The shape of the spectra are characterized by the slopes ($S1$, $S2$ & $S3$) derived after a second order polynomial fit in three different bands (see text)

Objects with high emission line features in their prism spectra show deviations larger than 10 sigma with respect to the "normal" values. Nevertheless, it does not exist an abrupt edge between normal and emission line spectra and, in addition, some objects can present a clear line produced by a plate blemish. Therefore, it is necessary to inspect some objects in order to retain a final list of candidates. We have inspected the spectra with a selector index greater than 4, that is, at least spectra with deviation greater than 2 sigma in two criteria or greater than

4 sigma in one of them. It has been necessary to inspect only some tens of objects in a graphic device, where a gray map and the extracted spectrum are available. This procedure provides a considerably reduced subset compared with the nearly $2\,10^4$ initial objects. Spectra showing a strong emission line produced by a plate blemish are easily recognized in the two-dimensional digitized image, and candidates have proved to have the highest values of our priority index. In Fig. 6 we present the prism spectra for the 11 selected candidates, and in Table 2 we show the differences, in sigma units, of the measured parameters R, $S2-S1$ and $S2-S3$, and the final selector index.

Table 2. ELGs candidates

Object Identifier	Log Flux	ΔR σ	$\Delta(S2-S1)\Delta(S2-S3)$ σ	σ	Selector Index
15586	4.792	16.2	12.2	11.7	40.1
2848	4.988	12.2	8.7	13.8	34.7
13394	4.902	4.4	8.6	9.5	22.5
11833	5.106	6.5	6.4	8.1	21.1
17066	4.728	7.8	4.1	5.1	16.9
10877	4.528	4.2	3.8	5.9	13.9
10143	4.503	5.2	0.0	4.9	10.2
9837	4.563	3.6	0.0	5.3	8.9
19406	4.760	0.0	3.9	4.3	8.2
19320	4.720	3.5	0.0	2.6	6.2
16021	4.969	2.1	0.0	3.5	5.6

5. Comparison with the visual sample

In order to test the reliability of the automatic procedure, the prism plate was carefully searched by visually scanning with a low-power binocular microscope by three independent observers, with a last review of all objects to derive a visual sample of candidates. We obtained a final list of 11 candidates. A total of 8 out of 11 candidates are in common with the automatically selected sample. A careful study of the objects missed in both searches enables us to understand the possible fails of the methods. With respect to the objects found only in the visual search:

- NGC 5789 (Sdm; m=14.2; size 0′.9×0′.8), with six visible HII regions, was no paired with their direct image due to its large extension, and, in consequence, not processed.
- NCG 5798 (Im; m=13.6; size 1′.4×1′.0), a bright and irregular galaxy showing five HII regions was lost in the automatic search. The reason is that the extracted prism spectrum concerns the central region of the galaxy, where no emission line is seen. In addition the spectrum is nearly saturated.
- The last remaining object was visually selected but was assigned only as probable candidate because it does not show a clear emission.

On the other hand, the three objects selected only in the automatic search were analyzed:

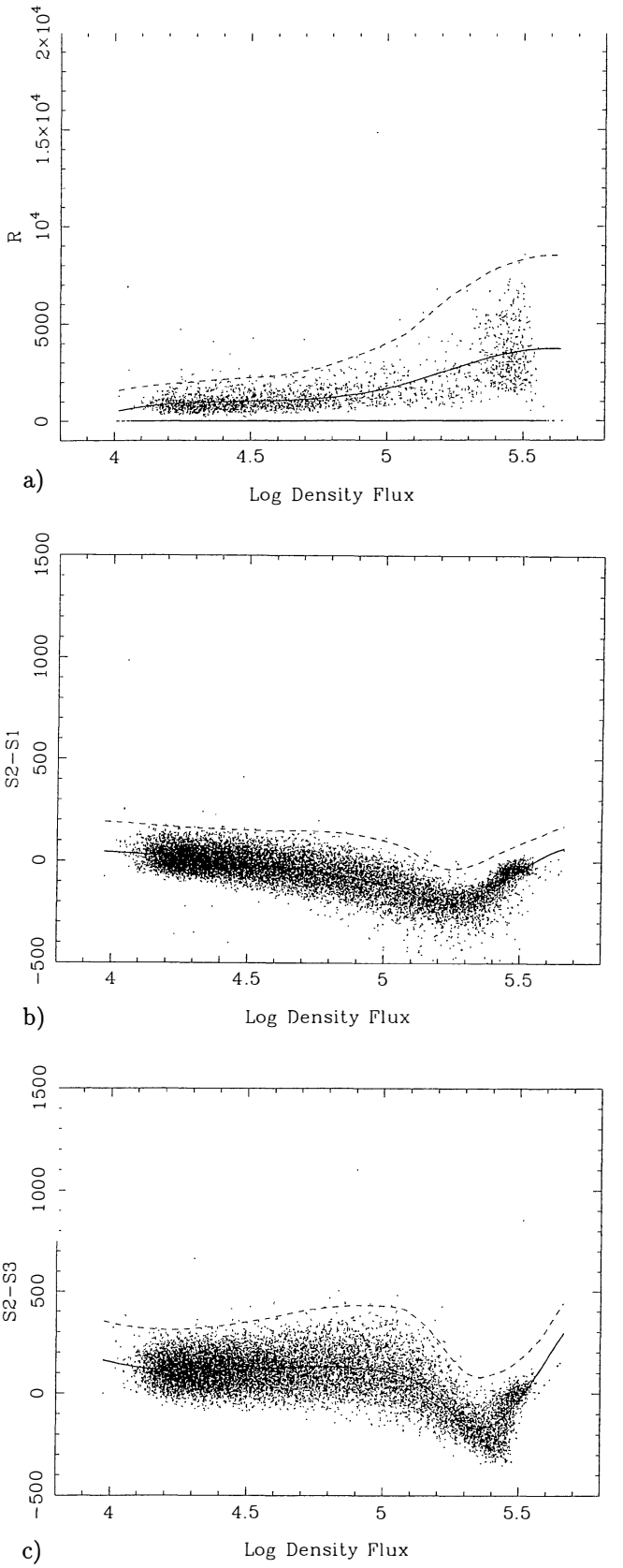

Fig. 5. Dependence of the residua after the continuum fit (R), and the slope variations ($S2-S1$) and ($S2-S3$) with the logarithm of the density fluxes. In each plot we have derived a curve following the general tendency (solid line). Dashed line shows the 3σ deviation curve

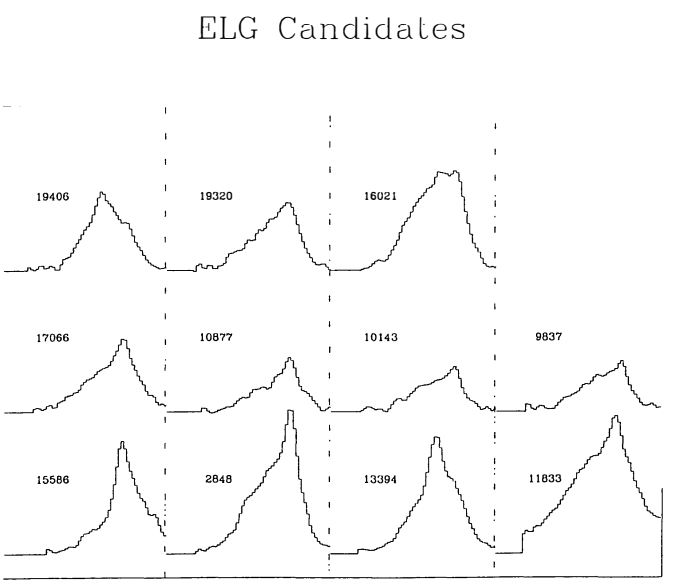

Fig. 6. Prism spectra of the final list of candidates

- #10877 exhibits a clear emission line and it should have been selected, pointing out a fail in the visual procedure.
- #10143 is very faint and its very weak emission-line feature in the digitized spectrum cannot be confirmed in the visual inspection of the plate.
- The emission feature in #19406 is abnormally shifted towards the blue region of the prism spectrum and, in addition, its appearance in the direct plate is stellar-like. It was not visually selected because it presented an anomalous shape, very different to that presented by typical ELG candidates.

So, we can resume that objects with strong lines in emission are not missed in the automatic search. Only bright and large galaxies with extranuclear emitting regions can be lost because of the fail of pairing algorithm or the presence of extranuclear emission. However, their large size and brightness assure them as known galaxies, and they can be recovered in a quick visual scanning of the plate.

6. Spectroscopic observations

The whole sample of 14 candidates selected both visually and automatically, with the exception of the two very bright and known galaxies NGC 5789 and NGC 5798, was observed in July 1994 with the IDS Spectrograph attached to the Cassegrain focus of the Isaac Newton Telescope at La Palma Observatory, Canary Islands, Spain. We used a TEK #3 CCD detector with equivalent pixel size of 24 μm, together with a 300 gr/mm grating, which provides a reciprocal dispersion of 3.3 Å/pixel and a spatial scale of 0.″71/pixel. The wavelength coverage was $\lambda\lambda$ 3600−7100 Å. The slit width was 4″ and the position angle was chosen to match the galaxy mayor axis when some elongated structure was apparent. Exposure times from 300 to 3600 s were taken according to the object brightness. Reduction of data was carried out using the ESO image processing software package (MIDAS), and involves flat-fielding, wavelength calibration, sky subtraction, extinction correction and conversion to absolute flux. The redshifts were measured using the strongest emission lines.

Figure 7 shows the 12 observed objects, together with their prism spectra. The first eight objects (Figs. 7a-h) were identified in both visual and automatic searches. The next three objects (Figs. 7i-k) were detected only in the automatic search, whereas the last one (Fig. 7l) was found only during the visual scan. In Table 3 we list the position, equivalent width and fluxes for the Hα+[NII] blend, the redshift and a preliminary spectral classification according to the visual inspection of the slit spectra. Also we list the designation and magnitudes for known objects, extracted from the NASA/IPAC Extragalactic Database (NED).

The eight objects identified in both searches display, all of them, strong emission lines in their slit spectra, and belong to different types of emission line galaxies. The strong emission line present in the prism spectra permits an easy detection. Two of the objects lost in the visual scan (#10877 & #10143) were confirmed as authentic ELG, whereas #19406 has proved to be a cool late type star with strong molecular bands and Hα in emission. These objects will be recognized in futures searches because they present stellar-like appearance in direct plate and they show the observed excess in the prism spectrum anomaly shifted to the blue part due to the combination of the Hα emission at zero redshift and the strong absorption. Finally, the object presented in Fig. 7l was lost in the automatic search, but spectroscopic observations show #05034 as a normal galaxy without Hα emission. This object was wrongly selected in the visual inspection because its prism spectrum presented a sharp profile.

7. Summary

A fully automatic procedure, developed to select ELGs candidates from the objective-prism plates of the UCM survey, has been presented. A prism plate and a direct plate, used mainly to distinguish between real objects and emulsion scratches, were scanned with the high performance MAMA machine. No density to intensity transformation has been necessary to identify the candidates, although some calibration will be necessary to extend this study and to estimate some physical parameters directly from the plates.

No spectral features are present in the prism spectra due to the reduced spectral range and low dispersion, and only the sharp red cut-off and the Hα line in emission are clearly seen. An automatic continuum fit algorithm has been developed and applied to all the spectra. Candidates are selected to present an anomalous high deviation over

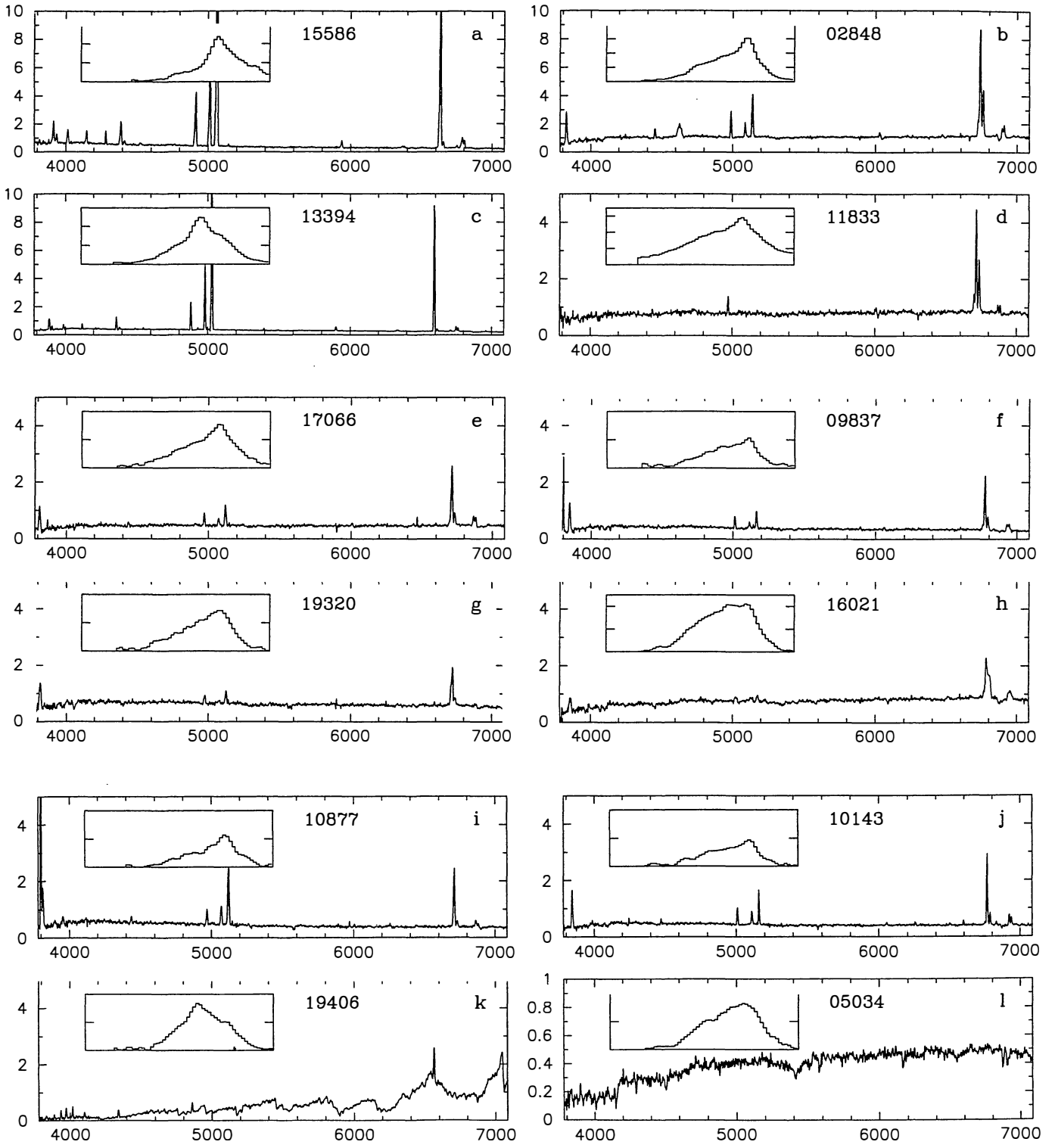

Fig. 7. Slit and prism spectra for the sample of candidates. For each object, the fluxes are given in units of 10^{-15} erg s^{-1} cm^{-2} $Å^{-1}$. Prism spectra cover from 6400 to 6850 Å

Table 3. Spectroscopic data

Object Identifier	(α,δ) (J2000.0)	Hα† Flux‡	Hβ	EW (Å) [OIII]λ5007	Hα†	z	Spectral Type*	Object	m
15586	14 54 12.0 +30 12 34	148.1	105	639	566	0.0107	HIIH	UGC 5988	
2848	15 08 42.6 +28 10 16	130.4	17	28	116	0.0264	HIIH	IRAS 15065+2821	15.3
13394	14 57 39.4 +26 39 53	77.5	50	317	318	0.0047	SS	NPM1G +26.0386	16.2
11833	14 59 34.3 +27 06 58	87.5	6	...	69	0.0226	SBN	UGC 09644	14.2
17066	14 52 22.8 +29 53 26	33.2	10	18	69	0.0225	HIIH	IRAS F14503+3005	
9837	15 00 53.1 +29 43 38	26.7	11	18	82	0.0316	SBN	CG 1277	18.0
19320	14 50 16.3 +28 24 38	24.8	7	8	45	0.0238	SBN		
16021	14 54 22.2 +27 42 04	43.8	5	5	49	0.0334	SBN	IRAS F14522+2754	16.6
10877	15 00 12.3 +28 08 53	27.5	13	48	72	0.0224	HIIH		
10143	15 00 55.6 +27 55 44	26.3	12	24	64	0.0307	HIIH		
19406	14 50 02.4 +27 52 03	...	...	...	...	...	Cool Star		
5034	15 05 33.8 +29 16 07	...	...	...	...	...	No Em.	NPM1G +29.0335	15.5

* According to Salzer et al. (1989). HIIH: HII Hotspot galaxies; SS: Sargent-Searle objects; SBN: Starburst nuclei galaxies.

† Hα fluxes and equivalent widths are referred to as the combined Hα+[NII] emission.

‡ Hα fluxes in units of 10^{-15} erg s^{-1} cm^{-2}

the continuum and/or strong discontinuities in the slopes of the extracted spectra calculated in three bands.

The results presented in the preceding sections demonstrate the consistency of our method against a visual procedure. All the objects detected visually have been recovered, and what is more important, there is a 20% of confirmed emission-line objects only detected through the automatic procedure. Only bright and extended objects with extranuclear HII regions can be lost, but their brightness and size assure them as known galaxies. The uncertainty introduced by wrong identifications (≈20% of plate blemish, scratches or no emission galaxies after a typical visual search; Zamorano et al. 1994) is notably reduced and the amount of beforehand information about each candidate is much bigger, including accurate astrometric positions (error < 1 arcsec).

All these advantages previously mentioned point definitively to the standard implementation of the automatic procedure for analyzing the raw data from Schmidt plates used during emission-line galaxy surveys. It is our intention to extend this work to a greater number of plates of our survey.

Acknowledgements. We would like to gratefully acknowledge the friendly assistance and warm hospitality received from the MAMA staff, and especially from Dr. Jean Guibert. We also express our thanks to the Calar Alto Observatory staff for their inestimable observing support, to M. Cordero, J. Gorgas and S. Pedraz for the first spectroscopic observations of candidates and to A.G. Vitores for useful suggestions and careful review of this paper. This work is based on observations collected at the German- Spanish Astronomical Center, Calar Alto, Spain, operated by the Max-Planck-Institut für Astronomie (MPIA), Heidelberg, jointly with the Spanish National Commission for Astronomy, and with the Isaac Newton Telescope, operated by the Royal Greenwich Observatory at the Spanish Observatory Roque de los Muchachos of the Instituto de Astrofísica de Canarias on behalf of the Science and Engineering Research Council of the United Kingdom and the Netherland Organization for Scientific Research. This work has made use of the NASA/IPAC Extragalactic Database (NED) which is operated by the JET Propulsion Laboratory, Caltech, under contract with the National Aeronautics and Space Administration. This work was supported in part by the Spanish "Programa Sectorial de Promoción General del Conocimiento" under grant No. PB93-456.

References

Birkle K. 1984, The Schmidt Telescope on Calar Alto, ed. Capaccioli, Proc. IAU coll. 78, Astronomy with Schmidt-Type Telescopes (Reidel, Dordrecht) 203

Boroson T.A., Salzer J.J., Trotter A. 1993, ApJ 412, 524

Borra E.F., Brousseau D. 1988, PASP 100, 1276

Borra E.F., Edwards G., Petrucci F. et al. 1987, PASP 99, 535

Clowes R.G., Emerson D., Smith M.G. et al. 1980, MNRAS 193, 415

Edwards G., Beauchemin M., Borra E.F. 1988, PASP 100, 266

Gallego J., Zamorano J., Rego M. et al. 1995, ApJ, in preparation

Guibert J., Moreau O. 1991, The Messenger 64, 69

Haro G. 1956, Bol. Obs. Tonantzintla Tacubaya 14, 8

Hewett P.C., Irwin M.J., Bunclark M.T. et al. 1985, MNRAS 213, 971

Horne K. 1986, PASP 98, 609

Infante L., Pritchet C.J. 1992, ApJS 83, 237

Jarvis J.F., Tyson J.A. 1981, AJ 86, 476

Kennicutt R.C., Kent S.M. 1983, AJ 88, 1094

Kennicutt R.C. 1992, A&A 388, 310

Kinman T.D. 1984, Searching for emission-line galaxies, ed. Capaccioli, Proc. IAU coll. 78, Astronomy with Schmidt-Type Telescopes (Reidel, Dordrecht) 409

Kunth D., Sargent W.L.W. 1986, ApJ 300, 496

Lipovetsky V.A. 1994, The importance of Wide-Field imaging, eds. H.T. MacGillivray et al., Proc IAU Symp. 161, Astronomy from Wide-Field imaging (Kluwer, Dordrecht) 3

MacAlpine G.M., Williams G. 1981, ApJS 45, 113

Markarian B.E. 1967, Astrofizica 3, 55

Markarian B.E., Stepanian J.A., Erastova L.K. 1987, The second Byuracan Spectral Sky Survey, eds. E.Ye. Khachikian et al., Proc. IAU Symp. 121, Observational evidence of activity in galaxies, p. 25

Maza J., Ruiz M.T., González L., Wichnjewsky M. 1989, ApJS 69, 349

Moreau O. 1992, PhD thesis, Université Paris 7

Moss C., Whittle M. 1993, ApJ 407, L17

Moss C., Whittle M., Irwin M.J. 1988, MNRAS 232, 381

Odewahn S.C., Humphreys R.M., Aldering G., Thurmes P. 1993, PASP 105, 1354

Rego M., Zamorano J., González-Riestra R. 1989, A&AS 79, 443

Reid N., Gilmore G. 1982, MNRAS 201, 73

Roeser S., Bastian U. 1991, PPM Star Catalog (Spektrum Akademischer Verlag, Heidelberg, Berlin, New York)

Salzer J.J., MacAlpine G.M., Boroson T.A. 1989, ApJS 70, 479

Schuecker P. 1993, ApJS 84, 39

Smith M.G. 1975, ApJ 202, 591

Surace C., Comte G. 1994, A&A 281, 653

Taff L.G., Lattanzi M.G., Bucciarelli B. 1990, ApJ 358, 359

Takase B., Miyauchi-Isobe N. 1993, Publ. Natl. Astron. Obs. Japan 3, 169

Véron P. 1986, in Structure and Evolution of Active Galactic Nuclei, ed. Guiricin et al. (Reidel, Dordrecht) 253

Wamsteker W., Prieto A., Vitores A.G. et al. 1985, A&AS 62, 255

West R.M. 1991, The Messenger 65, 45

Zamorano J., Rego M., Gallego J., Vitores A.G., González-Riestra R., Rodriguez-Caderot G. 1994, ApJS 95, 387

Zamorano J., Rego M., González-Riestra R., Rodriguez-Caderot G. 1990, Ap&SS 170, 353